

## CCD Imaging of the Inner Coma Jets of Comet P/Halley

James Boswell & David W. Hughes. *Department of Physics, University of Sheffield, Sheffield, S8 7RH, UK.*

**Abstract.** In this paper we analyse the inner coma section of a CCD image of comet P/Halley taken at 1807 UT on 1986 March 13th using a  $C_2$  filter (wavelength 5000 to 5200Å, half maximum) with the 3.8 m Anglo Australian Telescope at Siding Springs, Australia. Atmospheric turbulence leads to a spreading of the image detail and this produces a blander image of the inner coma region with a slower radial decrease of brightness in comparison to the unaffected image. We remove this smearing by utilising the point spread function of a star on the same CCD image. Jets were then revealed by removing the average background. Analysis of the jet structure enabled us to estimate the lower limit of the parent molecule velocity. This is found to be  $0.3 \text{ km s}^{-1}$ .

### Introduction

Within 2-3 AU of the Sun, sublimation of ice from active areas of cometary surfaces leads to the ejection of gas and dust in high velocity jets. These jets spread out to form a large, quasi-spherical cloud, known as the coma, which is, close to the Sun, typically  $10^5 \text{ km}$  across. The coma surrounds the small, solid nucleus and is responsible for scattering the majority of the incident sunlight.

This paper investigates the structure of these emissions using CCD images of comet P/Halley taken with a  $C_2$  filter (wavelength 5000 to 5200 Å, half maximum) at the prime focus of the 3.8 m Anglo Australian Telescope at Siding Springs, New South Wales. The image coma region corresponds to a square of side 20,400 km in the plane of the sky passing through the cometary nucleus, encompassing pixels 145 to 203 on the horizontal axis and pixels 264 to 322 on the vertical axis. In displaying the data it is sometimes helpful to plot brightness as a 'height' above the two dimensional pixel array. Using this convention the CCD image of the comet takes the form of a 'mountain' and it becomes convenient to extend the analogy and refer to brightness as height and small local intensity peaks as 'hillocks'.

### Overcoming the problem of atmospheric blurring of the CCD image

One of the major problems with ground-based astronomical images is distortion caused by atmospheric turbulence. The effect of the atmospheric turbulence is to independently smear out each of the point elements, which would make up the undistorted image, into a two-dimensional brightness pattern. Background stars can be regarded essentially as point sources. Hence, in an ideal image, they should appear as a single bright pixel. However, in reality, atmospheric blurring causes their image to be spread out over many pixels. Hence, in an image of the comet they appear as small hillocks on the surface of the overall mountain that represents the cometary brightness distribution. The height of a hillock above the background indicates the brightness of the star that it represents, and in order to ensure energy conservation, the total integrated height of the hillock (i.e. the sum of all the hillock  $DN$ -values) must equal the height of the equivalent point in the undistorted image. However, the shape of all the hillocks are the same, regardless of the brightness of the star that they represent. Clearly, every point element in the undistorted image has been affected in exactly the same manner as the background stars. Thus the final image is simply the superposition of all these resultant smeared intensity distributions. In mathematical terms, the original intensity distribution is convolved with a point spread function (PSF) that corresponds to the shape of the hillocks. Hence, it is theoretically possible to reconstruct the undistorted image using Fourier Transform Theory to deconvolve the PSF from the CCD image. Unfortunately, a secondary effect of the Fourier Transform method is to reduce the signal-to-noise ratio of the image. In the case of the P/Halley images it was found that, the S/N ratio was reduced to such an extent that the signal (undistorted image) became completely swamped by the noise. Thus, an alternative approach must be sought in order to deconvolve the comet image successfully.

### Image Deconvolution

The image of the comet can be more easily processed if the underlying Cartesian pixel array is replaced by an equivalent polar array which has the 'summit' of the mountain at the origin, and a radial pixel spacing that is the same as the original Cartesian spacing. The azimuthal spacing of the polar array should be chosen to ensure that there is no loss of resolution at the edges of the new image. Averaging the  $DN$ -values of all of the polar pixels for a complete azimuthal sweep then reduces the image to a one-dimensional brightness profile. Because of the inherent circular symmetry of the image, this average profile is a close approximation to any radial slice that is taken through the mountain. The same procedure may be applied to produce a brightness profile for a background star within the same field of view as

the comet. An approximate fit of the brightness profile of the comet may be obtained from the equation  $DN(R) = R^{-n}$  ( $R$  is the radial pixel number, where the central pixel in the image is numbered 1,  $DN(R)$  is its brightness and  $n$  may take any positive real number). However,  $n$  varies with  $R$  over a narrow range in the real profile, having values in the range 0 to 2. We can therefore generate a range of hypothetical brightness profiles for the cometary image by varying  $n$  between these limits. These hypothetical profiles are then convolved with the brightness profile generated for the background star, which acts as the PSF. The percentage change in brightness found on convolving the hypothetical profiles with the PSF may then be calculated.

It is found that this change is  $< 1\%$  for pixels where  $R > 10$  for all values of  $n$ , thus pixels with  $R > 10$  may be ignored in the subsequent selection of the value of  $n$  that will ultimately be used. For all pixels the change in brightness is negligible for  $0.25 < n < 0.40$ . With this information it is possible to select a value of  $n$  which produces a brightness profile which best matches that of pixels with  $r < 10$ . The value of  $n$  which provides the best fit for the data is 0.37, so a hypothetical brightness profile was generated from the equation  $DN(R) = R^{-0.37}$ , and this profile is then convolved with the PSF. We may then derive a percentage change in brightness between the original hypothetical profile with  $n = 0.37$  and the new profile after convolution. Each pixel of the original comet image can then be divided by the percentage change generated according to their equivalent  $R$ -value, in order to deconvolve the image.

Once the deconvolution has been performed, the integrated brightness of the deconvolved and the original images can be compared to assess the success of the operation. In this case, the integrated brightnesses were found to agree to within 1% over the complete image. The deconvolved image is shown in figure 1.

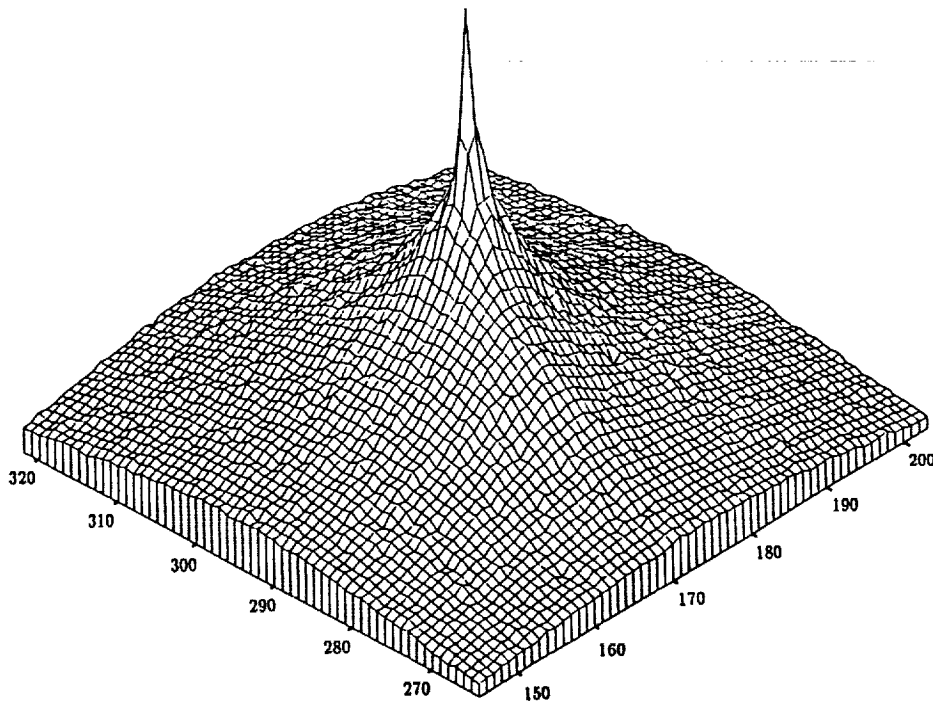


**Figure 1.** The deconvolved CCD image. The base grid represents the pixel array of the CCD image of comet P/Halley. The pixel numbers are shown. The vertical axis represents the deconvolved pixel  $DN$  value. Note the sharp peak at the central position i.e. at the nucleus. The base is at a  $DN$  'height' of 2460 with the peak at 12220.

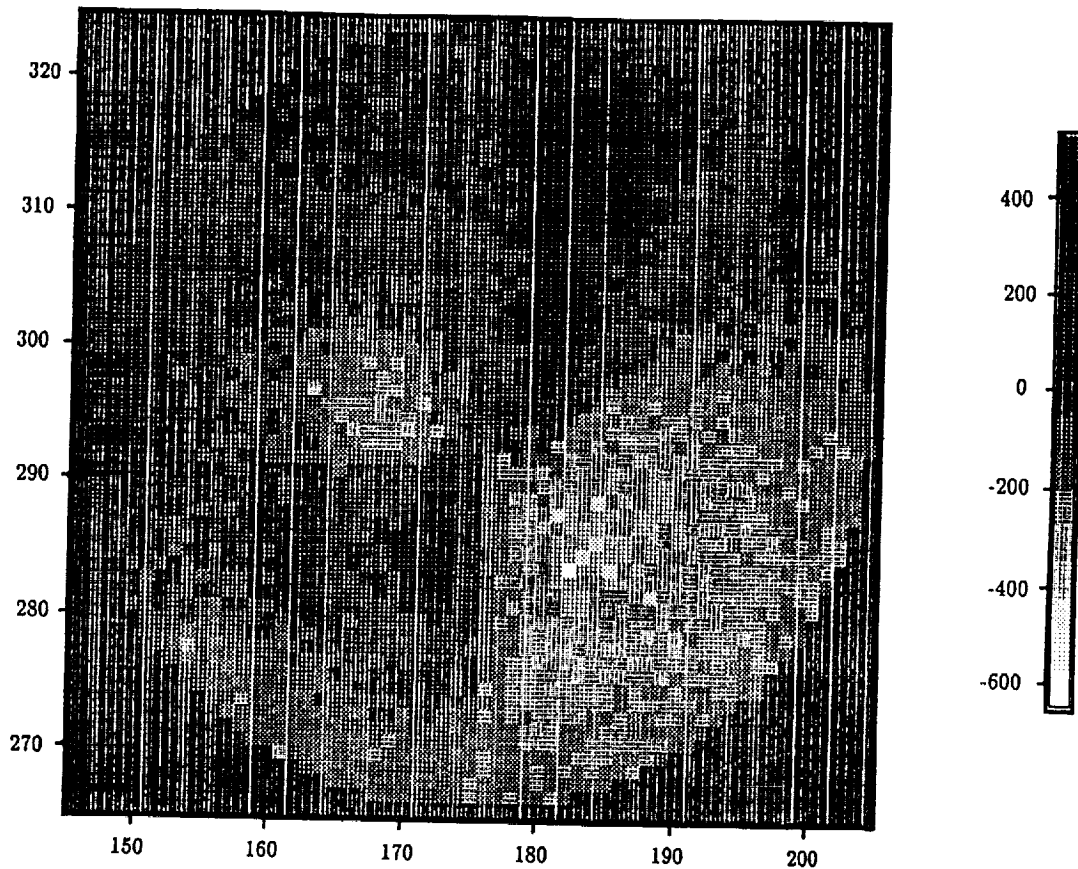


**Figure 2.** The deconvolved CCD pixel array with the average background removed. This is done by converting the pixel array from cartesian to polar coordinates, then finding the mean  $DN$  value over all  $\theta$  for each value of  $R$ , and subtracting this from all pixels at distance  $R$ . Note the two raised regions (jets). The  $C_2$  enhancement corresponds to, at maximum 9%.

### Enhancing Image Detail

Once the image had been deconvolved, the average background brightness was removed. This was achieved by subtracting the average brightness profile, generated in the conversion from cartesian to polar coordinates, after deconvolution, from each pixel according to its  $R$ -value. Plotting the data as a greyscale map revealed two jets in the image (figure 2). This method of detail enhancement has been used previously by A'Hearn (1986).

### Calculating Jet Velocity

By investigating the structure of the jets it is possible to make an estimate of the outflow velocity assuming that the effect of solar radiation pressure is negligible and that the outflow velocity is constant. If we adopt a 'lawn-sprinkler' model (Larson and Minton, 1972) to account for the curvature of the jets, the enhanced image may be reconstructed in 'quasi-polar' form such that radial displacement is displayed on the ordinate and azimuthal displacement is displayed on the abscissa (figure 3). Using this format the degree of curvature can be assessed from the angle of slope of the jets, which now form straight ridges across the image. Given the rotation period of P/Halley, a lower limit estimate of the outflow velocity can be made.

Unfortunately the rotation period of P/Halley is still the subject of investigation. Itoh (1985) first discovered a 2.2 day periodicity, but within a year Millis and Schleicher (1986) added a 7.4 day periodicity. Subsequent analysis supports both periods, leaving the issue unresolved. For the purpose of calculating the outflow velocity of the jets,  $v_G$ , the 7.4 day period provides a lower limit,  $v_G \geq 0.1 \text{ km s}^{-1}$ . If the 2.2 day period is proved correct, however, this limit may be raised to  $v_G \geq 0.3 \text{ km s}^{-1}$ .

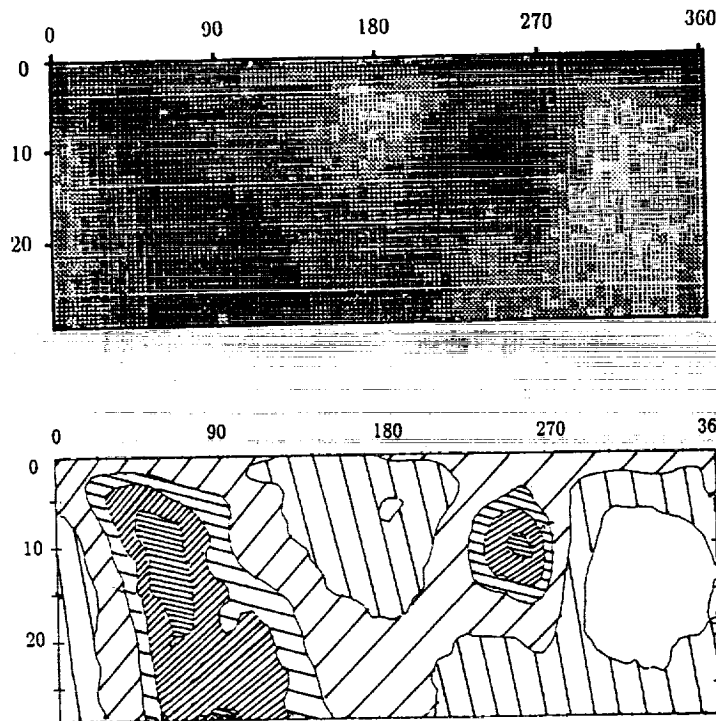


Figure 3. Both figures are essentially figure 2 redrawn with the abscissa representing the azimuthal distance  $\theta$ , and the ordinate representing the radial pixel distance  $R$ . The grey scale used in the upper plot is the same as that used in figure 2. The lower plot has contours at -450, -250, -50, 150, 250 and 350. The degree of curvature of the jets can be assessed from their gradient on this plot.

### References

- A'Hearn, M.F., Hoban, S., Birch, P.V., Bowers, C., Martin, R., Klingsmith III, D.A., 1986. *Nature*, **324**, 649-651.  
 Larson, S.M., and Minton, R.B., 1972. *Comets: Scientific Data and Missions*, Kuiper, G.P., and Roemer, E., 183-208.  
 Itoh, T., 1985. *IAU Circ*, **4155**  
 Millis, R.L., and Schleicher, D.G., 1986. *Nature*, **324**, 646-649.